Chem

CellPress

Article

Gigantic Porphyrinic Cages

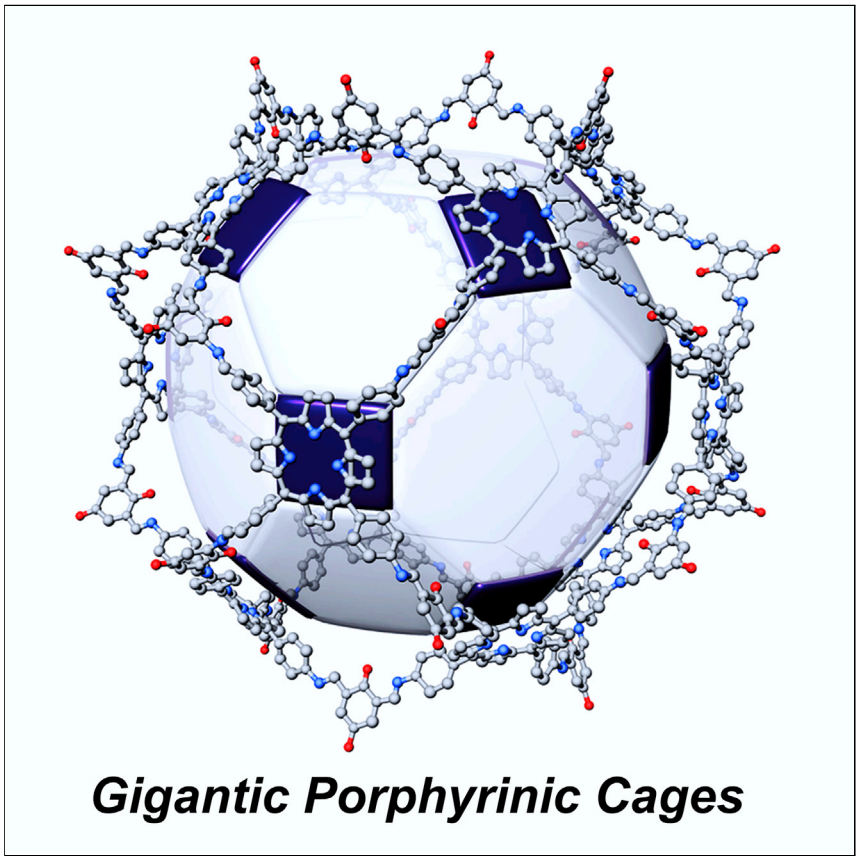

Jaehyoung Koo, Ikjin Kim, Younghoon Kim, ..., Seungha Kim, Mu-Hyun Baik, Kimoon Kim

mbaik2805@kaist.ac.kr (M.-H.B.)
kkim@postech.ac.kr (K.K.)

HIGHLIGHTS

One-pot, template-free synthesis of gigantic porphyrinic cages mimicking COPII protein

Atomic resolution X-ray crystallographic analysis of $P_{12}L_{24}$

Efficient photooxidation under heterogeneous catalytic setting

Guest molecule insertion inside Zn-metallated $P_{12}L_{24}$

Porphyrin-based 3D molecular architectures encompassing a confined internal void have comparatively been less explored, despite their potential benefits. Here, we report a rational one-pot, template-free strategy for constructing a 5.3 nm porphyrin-based gigantic organic cage $P_{12}L_{24}$, which is reminiscent of the structure of COPII protein cuboctahedral cages. To the best of our knowledge, this is the largest purely organic cage reported so far. $P_{12}L_{24}$ efficiently catalyzes the photooxidation of dihydroxynaphthalene derivatives, thereby confirming the benefit of these gigantic structures with mesoscopic channels. Furthermore, we demonstrate the insertion of a long pillar linker (~4 nm in length) into Zn-$P_{12}L_{24}$ in solution. We believe that our strategy may establish a new direction toward the construction of higher level, covalently bonded multiporphyrinic cages.

Koo et al., Chem 6, 1–11
December 3, 2020
https://doi.org/10.1016/j.chempr.2020.10.002

Please cite this article in press as: Koo et al., Gigantic Porphyrinic Cages, Chem (2020), https://doi.org/10.1016/j.chempr.2020.10.002

Chem

CellPress

Article

Gigantic Porphyrinic Cages

Jaehyoung Koo,[1,2,6] Ikjin Kim,[1,3,6] Younghoon Kim,[1] Dasol Cho,[4,5] In-Chul Hwang,[1] Rahul Dev Mukhopadhyay,[1] Hayoung Song,[1] Young Ho Ko,[1] Avinash Dhamija,[1] Hochan Lee,[1,3] Wooseup Hwang,[1] Seungha Kim,[4,5] Mu-Hyun Baik,[4,5,*] and Kimoon Kim[1,2,7,*]

SUMMARY

Due to the existing challenges in the synthesis of covalently linked large organic cages, the potential benefits of such gigantic structures have been less explored, comparatively. Here, we present a one-pot, template-free strategy to construct a porphyrin-based gigantic organic cage $P_{12}L_{24}$, built with 12 square-shaped porphyrins (P) and 24 bent linkers (L). Single crystal X-ray analysis of $P_{12}L_{24}$ revealed a cuboctahedron structure with a diameter of ~5.3 nm reminiscent of the COPII protein with a cuboctahedral geometry. To the best of our knowledge, it represents the largest, pure organic synthetic cage reported so far. By virtue of its large voids facilitating mass transport of substrates, 3a efficiently catalyzes the photooxidation of dihydroxynaphthalene derivatives in a heterogeneous setting, corroborating the benefits of these structures. Additionally, we demonstrate the insertion of a linear guest molecule into Zn-metallated cage Zn-3b in solution, which may facilitate the synthesis of multivariate gigantic cages in the future.

INTRODUCTION

Mother nature has constantly inspired chemists to construct and mimic the functioning of complex and challenging chemical architectures and to explore them for a wide variety of emergent applications. For instance, the wheel-like macrocyclic systems in natural light-harvesting antenna complexes, which consist of an ordered array of chlorophyll molecules and other pigments embedded in the thylakoid membrane absorb photons and deliver energy to the photosynthetic reaction center with an efficiency greater than 95%.[1] Another prominent example is that of the gigantic hollow assemblies, such as ferritin, coat protein complex II (COPII) cage, and various virus capsids composed of biomacromolecules, known for functions such as secure encapsulation of genetic material and storage.[2–8] Nature manages to precisely construct these aesthetic structures aided by a highly efficient bottom-up self-assembly process, which has also been a promising strategy and tool for supramolecular chemists to synthesize complex nanoarchitectures. In these aspects, chemists have been exploring challenging synthetic pathways to build various porphyrin-based architectures, such as dendrimer, 2D nanorings, and 2D/3D infinite frameworks.[9–18] Among these, cage-like 3D architectures, which possess an inherent internal void encompassed by multiporphyrin units, combine the features of both types of the aforementioned natural assemblies. As a result, they have received considerable attention as they can be utilized in a wide variety of applications, including light-harvesting,[19,20] guest encapsulation,[21] enzyme-like catalysis,[22] ion transport,[23] etc. So far, the 3D cage-like structures comprising more than 3 porphyrin units have been mostly synthesized by utilizing non-covalent interactions.[19,20,24–27] For instance, Nitschke and co-workers synthesized tetrahedron or

The Bigger Picture

A bottom-up self-assembly process has been a promising tool to mimic structurally complex natural architectures, e.g., the bacteriochlorophyll-based macrocyclic arrays in natural light-harvesting systems and gigantic hollow assemblies, such as ferritin, COPII cage, and other viral capsids. Nevertheless, there is still a long way to go before we can astutely program multiple building blocks to form predesigned structures. In this context, the reported examples related to atomically precise multiporphyrinic arrays and cages are limited by their tedious synthesis, poor yield and solubility, atomic-scale characterization, and small-sized cavities. Here, we report a strategy to synthesize gigantic porphyrinic cages (~5.3 nm) with 36 components and demonstrate its potential applications in processes such as heterogeneous photocatalysis and guest encapsulation. Our strategy may establish a cornerstone toward the construction of higher level, covalently bonded multiporphyrinic molecular containers.

cube-shaped multiporphyrinic metal-organic cages and explored their applications.[21,28–34] In contrast, however, the synthesis of covalently linked 3D multiporphyrinic cages has been comparatively less explored and was achieved only via tedious synthetic routes and template-assisted strategies, limiting the scope of their applications.[35–38] Therefore, although it is desirable to develop a template-free, one-pot synthesis of such 3D cage-like multiple (more than three) porphyrin assemblies using a covalent strategy, it remains challenging.

One strategy to the one-pot synthesis of organic cages is to utilize dynamic covalent chemistry (DCC), as demonstrated by Cooper and others.[39–51] In this DCC strategy, single or multi-component approaches, typically using two-way and three-way connecting building blocks, [2n + 3n] have been employed. However, these approaches usually lead to the formation of small-sized organic cages (cavity diameter < 2 nm), thereby restricting their applications. So far, one of the rare successful examples is the synthesis of a [8 + 12] boronic ester cage (~3 nm in diameter) reported by Mastalerz and co-workers in 2014.[46] In another report, single-component approach based on reversible trimerization of diboronic acid successfully produced a boroxine cage (~2.5 nm diameter) (n = 12), but failed to produce a larger cage (n = 30).[48] Thus, the synthesis of larger sized (> 3.1 nm) cages with a higher order of the [2n + 3n] approach (n > 4) or single-component approach (n > 20) remains challenging. One reason is that entropy favors the formation of a larger number of smaller cages over a smaller number of larger cages during the self-assembly process.[47,51] Another important issue is the low solubility of oligomeric intermediates and undesired polymeric side products, which prevent them from further participation in the dynamic, reversible process leading to the desired thermodynamic products.[52] Therefore, to successfully synthesize a large organic cage, it is important to circumvent these synthetic obstacles by a judicious design of the cage components.

In 2015, we reported porphyrin boxes (PBs), which are rationally designed covalent organic cages consisting of six porphyrin units (**P**) and eight triamine linkers (**L**) ($\mathbf{P_6L_8}$), with a rhombicuboctahedron geometry.[53] The hollow nature of PBs in combination with fascinating properties of the porphyrin units led us to explore a wide range of their applications, including ion channel, electrocatalysis, and construction of hierarchical superstructures.[23,54–57] Encouraged by the successful synthesis of PBs, we set out to construct larger porphyrin-based organic cages. Inspired by the elegant works of Fujita and co-workers,[58–63] we envisioned that a [2n + 4n] DCC approach using a porphyrin derivative (P) as a 4-connecting square-shaped building unit and a bent, 2-connecting linker (L) with a suitable length and bent angle would produce a series of porphyrin-based large cages ($\mathbf{P_{12}L_{24}}$, $\mathbf{P_{24}L_{48}}$, $\mathbf{P_{30}L_{60}}$, …) (Figure S4; Table S1). Among these, we set the $\mathbf{P_{12}L_{24}}$ as our first target, which could be a structural model of the transport protein complex COPII, with an elegant cuboctahedral architecture. COPII plays an essential role in the cellular machinery, accommodating cargoes of different shapes and mediating their transport from the endoplasmic reticulum.

Herein, we report a rational one-pot synthesis of a gigantic porphyrin-based organic cage, $\mathbf{P_{12}L_{24}}$ (**3a** and **3b**), consisting of 12 porphyrin units with an outer dimension of ~5.3 nm and an inner cavity of ~4.3 nm in diameter, via template-free dynamic covalent self-assembly (Scheme 1). The self-assembly involves 36 building blocks emerging into a large cage through the formation of 48 new covalent bonds. The structure of **3a** has been unequivocally determined at atomic resolution using single crystal X-ray crystallography, despite it containing only light atoms with tremendous void resulting in low intensity and poor resolution of X-ray diffraction. To the best of

[1]Center for Self-Assembly and Complexity (CSC), Institute for Basic Science (IBS), Pohang 37673, Republic of Korea

[2]Department of Chemistry, Pohang University of Science and Technology (POSTECH), Pohang 37673, Republic of Korea

[3]Division of Advanced Materials Science, Pohang University of Science and Technology (POSTECH), Pohang 37673, Republic of Korea

[4]Center for Catalytic Hydrocarbon Functionalizations, Institute for Basic Science (IBS), Daejeon 34141, Republic of Korea

[5]Department of Chemistry, Korea Advanced Institute of Science and Technology (KAIST), Daejeon 34141, Republic of Korea

[6]These authors contributed equally

[7]Lead Contact

*Correspondence: mbaik2805@kaist.ac.kr (M.-H.B.), kkim@postech.ac.kr (K.K.)

https://doi.org/10.1016/j.chempr.2020.10.002

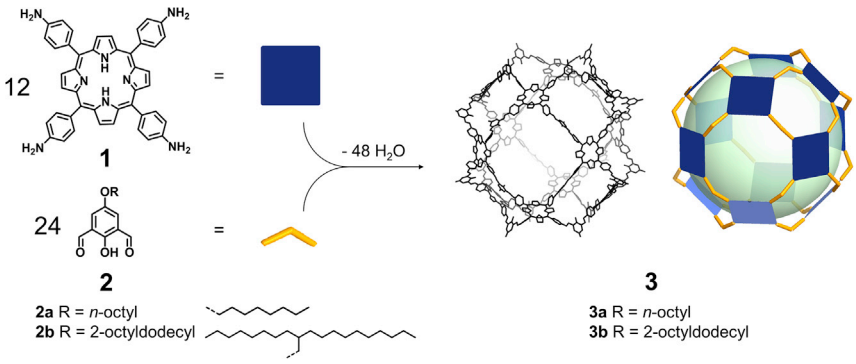

Scheme 1. Design and Synthesis of the Gigantic Porphyrinic Cages $P_{12}L_{24}$

our knowledge, this is the largest, purely organic cage reported so far. To validate the solid-state applications, we demonstrated a high heterogeneous catalytic activity of **3a** in the photooxidation of dihydroxynaphthalene derivatives, confirming the benefits of a gigantic structure with a mesocellular, hollow nature. Furthermore, we also demonstrated precise installation of a long pillar linker within Zn-metallated **3b**, suggesting the potential utility of such an extremely large synthetic molecular container for the encapsulation of large guest molecules.

RESULTS AND DISCUSSION

Design and Synthesis of Porphyrin-Based Large Organic Cages

At the outset of this work, we carried out a modeling study to screen several ditopic linkers with different lengths but with a fixed 120° bent angle, suitable for the formation of $P_{12}L_{24}$. The results suggested that the formation of cages with relatively short linkers would be thermodynamically favorable (Table S1) compared with those with longer linkers. Hence, we chose 2-hydroxy-1,3-benzenedicarboxaldehyde derivatives, which are short and rigid linkers with limited bond rotation to serve our purpose (Scheme 1).[43,47,49]

Stirring of a mixture of square-shaped tetra(4-aminophenyl)porphyrin (**1**) and two equivalents of bent-shaped 2-hydroxy-5-octyloxy-1,3-benzenedicarboxaldehyde (**2a**) in dry 1,2-dichlorobenzene (*o*-DCB) at room temperature for 3 days produced a crystalline product, $P_{12}L_{24}$ (**3a**), in 17% yield. MALDI-TOF (matrix-assisted laser desorption/ionization time-of-flight) mass spectrometry revealed a single peak at m/z = 13,913, corresponding to the $[M+H]^+$ ion of **3a** consisting 12 porphyrin units and 24 bent linkers, with a molecular formula of $C_{912}H_{841}N_{96}O_{48}$ (Figure S6). The FTIR spectrum of **3a** also clearly showed the emergence of imine C=N stretching bands at 1,625 and 1,577 cm^{-1} (Figure S12). Unfortunately, **3a** was not soluble enough to be characterized by solution-state NMR studies. To overcome the solubility issue, another cage molecule **3b** decorated with long branched alkyl chains was synthesized using 2-hydroxy-5-(2-octyldodecyl)oxy-1,3-benzendicarboxaldehyde (**2b**), instead of **2a** (Scheme 1). As expected, **3b** showed an improved solubility in organic solvents as compared with **3a**, making it suitable for solution-state characterization. The ^1H NMR spectrum of **3b** was relatively simple, reflecting its highly symmetric structure (Figures 1A, and S1–S3). The spectrum also confirmed the absence of any free aldehyde group of the ditopic linker. Furthermore, the formation of intramolecular hydrogen bonds in the salicylimine linkages was evident from the deshielding in the chemical shift of the hydroxyl protons, *e* (Figure 1A).[44] Additionally, the FTIR spectrum of **3b** showed strong bands at 1,625 and 1,579 cm^{-1}, corresponding to the C=N stretching (Figure S13). Diffusion-ordered

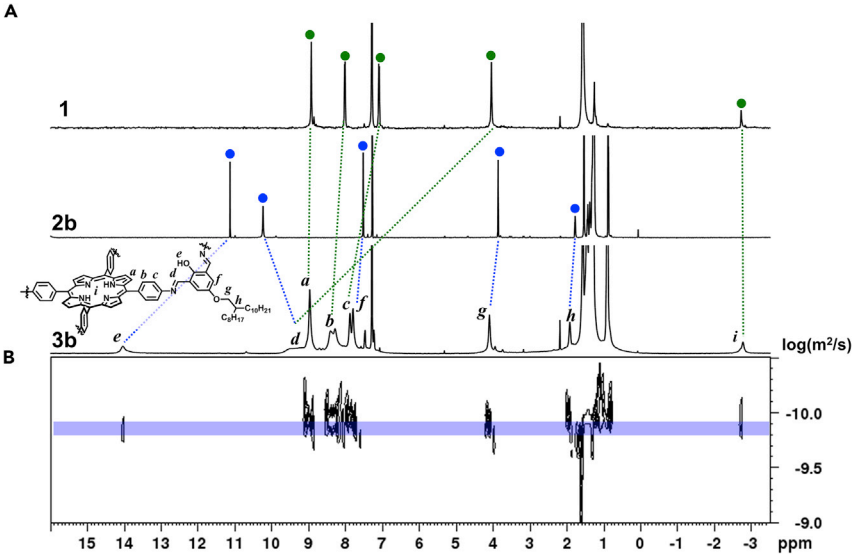

Figure 1. NMR Characterization of 3b

(A) ^{1}H NMR spectra of **1**, **2b**, and **3b**.

(B) DOSY NMR spectrum of **3b**.

spectroscopy (DOSY) NMR (Figure 1B) showed that all signals shared the same diffusion coefficient ($D = 1.17 \pm 0.07 \times 10^{-10}\ m^2\ s^{-1}$) at 25 °C in $CDCl_3$, confirming the existence of a single species in solution. The corresponding hydrodynamic radius (R_{hyd}) calculated by the Stokes-Einstein equation was 3.44 ± 0.02 nm, which matched well with the expected dimensions of the cage and the X-ray crystal structure of **3a** (*vide infra*). However, the ^{13}C NMR spectrum of **3b** was not sensitive enough for further characterization. The ^{13}C magic-angle spinning (MAS) solid-state NMR spectra of **3a** and **3b** were therefore recorded (Figure S5), and the signals were compared with the solution-state ^{13}C NMR spectrum of a model compound (Scheme S6). Signals from both the aromatic and aliphatic units of **3a** and **3b** matched well with those of the model compound. Further characterization of **3a** was conducted by AFM measurements, employing a drop-casting method of a highly diluted solution of **3a** on a freshly cleaved mica substrate (Figure S9). The height of each bright spot was found to be around 4 nm, which matched the expected diameter of a single **3a** molecule.

X-Ray Crystallographic Analysis

After numerous unsuccessful attempts, the structure of **3a** has been unequivocally confirmed by single crystal X-ray crystallography. It was challenging to obtain high-quality X-ray diffraction data, as the structure of **3a** possessed an enormous void space without heavy metal atoms, resulting in a low resolution and weak intensity of X-ray diffraction (Figure S18B). Large single crystals (~80 μm, Figure S18A) of **3a** were grown by slow vapor diffusion of isopropanol into chlorobenzene solution, and X-ray diffraction data for **3a** were collected to 2.1 Å resolution using synchrotron radiation.

3a crystallized in the tetragonal space group, *I*4/*m*, with two molecules in the unit cell. As expected, **3a** exhibited a truncated cuboctahedron structure (Figure 2B), with an outer diameter of 5.3 nm (Figure 2A), maximum ~7.0 nm, including alkyl chains (the positions of the alkyl chains were assigned by assisted of powder X-ray analysis, Figure S19). The overall structure is reminiscent of that of the cuboctahedral transport protein cage COPII,[5,6,64] which consists of heterotetrameric units and

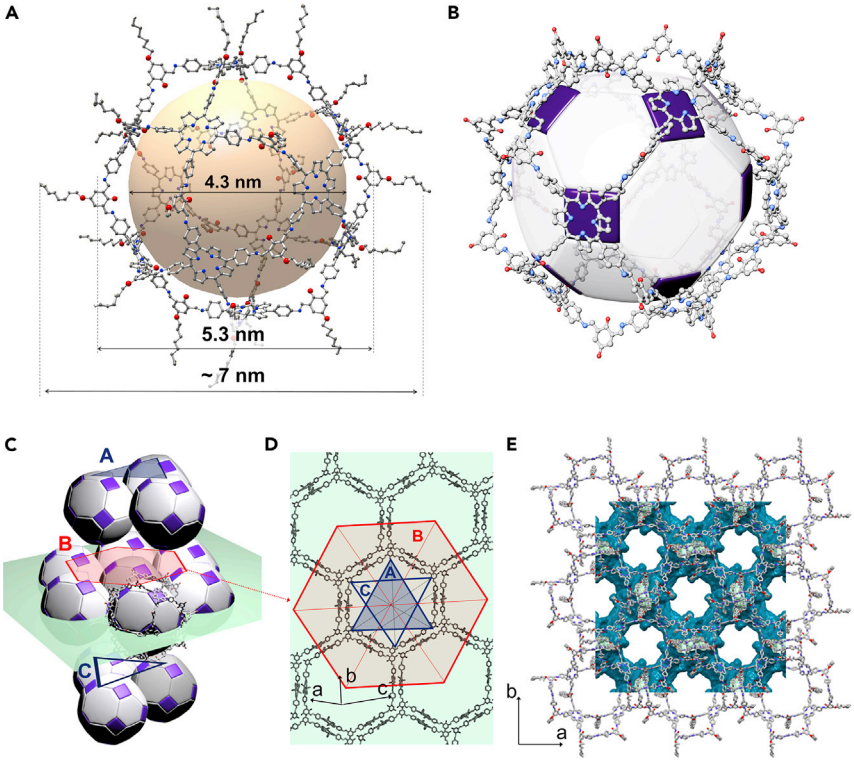

Figure 2. Crystal Structures of 3a

(A and B) (A) Crystal structures of **3a** with ball and stick model and (B) overlapped with truncated cuboctahedron 3D model of **3a** (with C, N, and O represented as gray, blue, and red balls, respectively).

(C and D) (C) The face-centered cubic ABC packing model of **3a** and (D) the sliced image of the closely packed **3a** crystal structure.

(E) The view down the *c* axis of **3a** revealing large channels, where the blue surface represents a solvent-accessible surface with a probe radius of 1.7 Å. Hydrogen atoms are omitted for clarity.

other coat components meeting at the tetrameric vertex similar to **1** and **2a**, respectively, as we observed in the X-ray structure of **3a**. The minimum inner diamter of the large cavity is around 4.3 nm, considering Van der Waals radius (from center of porphyrin units to the opposite end, Figures 2A and S20). To the best of our knowledge, this is the largest pure organic cage reported thus far (Figure 2A). A close inspection of the crystal structure of **3a** revealed that four porphyrins arranged along the mirror plane, perpendicular to the central 4-fold axis, were connected only via anti-conformation of the imine linkage, whereas the remaining 8 porphyrins, residing on both sides of the aforementioned mirror plane were connected by imine linkages with a mixed conformation (*syn*: *anti* = 3:1; Figures S21 and S22). In solution, however, rapid interconversion between the *syn*- and *anti*-conformations of the imine linkages in the cage molecule may occur as indicated by the rather broad and symmetric nature of the solution-state NMR spectrum of **3b** (Figure 1A).

In the crystal structure, the cage molecules were closely packed in a face-centered cubic manner with the generation of octahedral and tetrahedral extrinsic voids (2.2 and 1.6 nm in diameter, respectively, Figures 2C and S23). The adjacent cages interacted via slightly slipped, face-to-face (porphyrin-porphyrin) stacking (distance, 3.7 Å), and C–H···π weak hydrogen bond between the alkyl chains and the salicylic units (Figure S25). The resulting arrangement of **3a** led to the formation of open

channels along the *c* axis ([110] plane) with dimensions of ~24 × 18 Å (Figures 2E and S24). Because of its hollow nature and the absence of metal atoms, **3a** possesses the lowest density (calculated density, ~0.29 g/cm^3) and the highest solvent-accessible volume (~75.4%) among molecular crystals.[65]

Although we have tested various soft activation methods (solvent exchange, supercritical CO_2 activation, liquid ethane activation, etc.), subsequent gas sorption experiments showed that activated **3a** adsorbed only a small amount of N_2 up to 400 cm^3/g at 77 K (Figure S26), with a hysteresis in the sorption isotherm in the region between 0.4~0.7 P/P$_0$. The powder X-ray diffraction profile of activated **3a** (Figure S27) exhibited significant broadening and shifting of the peaks, indicating collapse of the packing structure and/or deformation of the cage structure upon activation, which is presumably responsible for the low gas sorption.

Heterogeneous Photocatalysis

Since crystalline **3a**, once formed, was sparingly soluble in common solvents but maintained its structure in the presence of solvent molecules, we decided to investigate the photocatalytic activity of the large cage in solution in a heterogeneous setting. Photooxidation of 1,5-dihydroxynaphthalene (DHN) in acetonitrile was studied in the presence of crystalline **3a**, monomeric porphyrin **PM** (Scheme S7), or porphyrin box **PB-1**[55] (Figure S28) as a heterogeneous catalyst (Figure 3). In each case, upon irradiation (> 420 nm), an increase in absorbance at ~420 nm was observed, indicating the generation of the oxidized product, juglone (Figures S29 and S30). However, the photocatalytic conversion with **3a** was much faster than that with **PB-1** and **PM** (Figure S29D). Furthermore, the photooxidation of modified DHN derivatives consisting of bulky 4-(*tert*-butyl)phenyl and 4-(pentyloxy)biphenyl groups in the 2- and 6-positions (DHN-b and DHN-c, respectively) also exhibited a higher photocatalytic performance for **3a** than that of **PB-1** (Figures 3B, 3C, and S32–S34). The difference between **3a** and **PB-1** in the catalytic conversion rate was more prominent when larger substrates (DHN-b and DHN-c) were employed. We further studied the effect of grinding of the **3a** crystals on their photocatalytic performance. The results were not significantly different, which means that the external surface of the crystals did not play a crucial role in the catalytic reaction when compared with the internal cavity of the cage (Figure S31). These observations can be attributed to the larger voids and channels of **3a**, which could enhance the diffusion of larger substrates and products. It may be noted that the catalytic oxidation was observed only upon excitation with a visible light source (Figure S36).

Encapsulation of a Guest Molecule

To further verify the size of the internal cavity of the large organic cages as well as to explore the scope of guest encapsulation in the solution state, we carried out the insertion of a pyridine terminated linker, which might coordinate with the porphyrinatozinc(II) moieties at the opposite ends of Zn-metallated **3b** (distance, ~4.3 nm), across the cavity (Figure 4A). We first performed Zn^{2+}-metallation of the porphyrin units of **3b** (Zn-**3b**) using a standard procedure and characterized it by MALDI-TOF, UV spectroscopy, and ^{1}H NMR (Figures 4B, S7, S8, and S38). For the linker insertion experiments, Zn-**3b** was prepared *in situ*, followed by systematically titrating it with a solution of the long pillar linker in $C_2D_2Cl_4$. As anticipated, NMR investigations suggested that a linear linker (**4**) with an appropriate length (~3.9 nm) was suitably inserted and precisely positioned within the Zn-**3b** (Figures 4B and S39) acting as a molecular ruler spanning the internal cavity of the cage. Unequivocal assignment of the ^{1}H NMR signals was achieved by conducting several 2D NMR

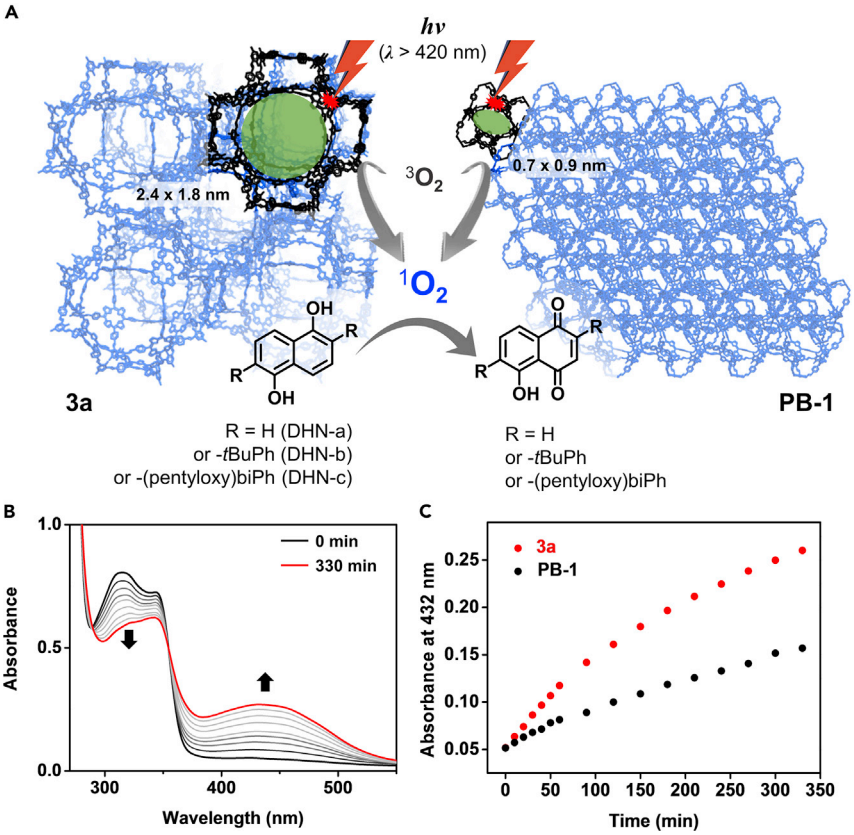

Figure 3. Photooxidation of DHN Derivatives Catalyzed by 3a

(A) Scheme for the photooxidation of DHN derivatives using **3a** or **PB-1**.

(B) Photooxidation of DHN-*t*BuPh (DHN-b) catalyzed by **3a** in the presence of oxygen and visible light irradiation (λ > 420 nm).

(C) Comparison of photocatalytic performance of **3a** (red) and **PB-1** (black) for the oxidation of DHN-b as a function of time.

experiments (^{1}H-^{1}H COSY (homonuclear correlation spectroscopy), NOESY (nuclear Overhauser effect spectroscopy), ^{1}H-^{13}C HSQC (heteronuclear single quantum coherence spectroscopy); Figures S40–S46). The ^{1}H NMR spectrum of a 1:1 mixture of **4** and Zn-**3b** in $C_2D_2Cl_4$ displayed several features consistent with the formation of **4**⊂Zn-**3b** in solution. In particular, the α-pyridyl proton ***i*** of **4**, which is now in a close proximity to the porphyrinatozinc(II) moieties upon the internal coordination, showed the largest upfield shift (8.69 to 2.26 ppm), which is in accordance with previous literature reports dealing with similar systems (Figure 4B).[18] Furthermore, a cross peak in the NOESY spectrum, signaling the NOE between the proton of the α-pyridyl proton ***i*** of **4** and the porphyrinatozinc(II) proton ***a*** (Figure S40), confirmed the coordination assisted insertion of **4** within Zn-**3b**.[66] DOSY experiments further corroborated the presence of [**4**⊂Zn-**3b**] in solution (Figure 4C). In the DOSY spectrum, both **4** and Zn-**3b** diffused at the same rate, which indicated a strong evidence that **4** was inserted inside the internal cavity of Zn-**3b**. The DOSY spectrum of control mix clearly contained two independent molecules that diffused separately (Figure S47C). The binding affinity of Zn-**3b** for **4** in $C_2H_2Cl_4$ was measured to be 1.4×10^7 M^{-1} by UV-vis titration (Figure S48). This proof-of-concept demonstration of guest encapsulation can lead to the preparation of multivariate gigantic cages containing precisely positioned functionalities inside their large cavities, such as

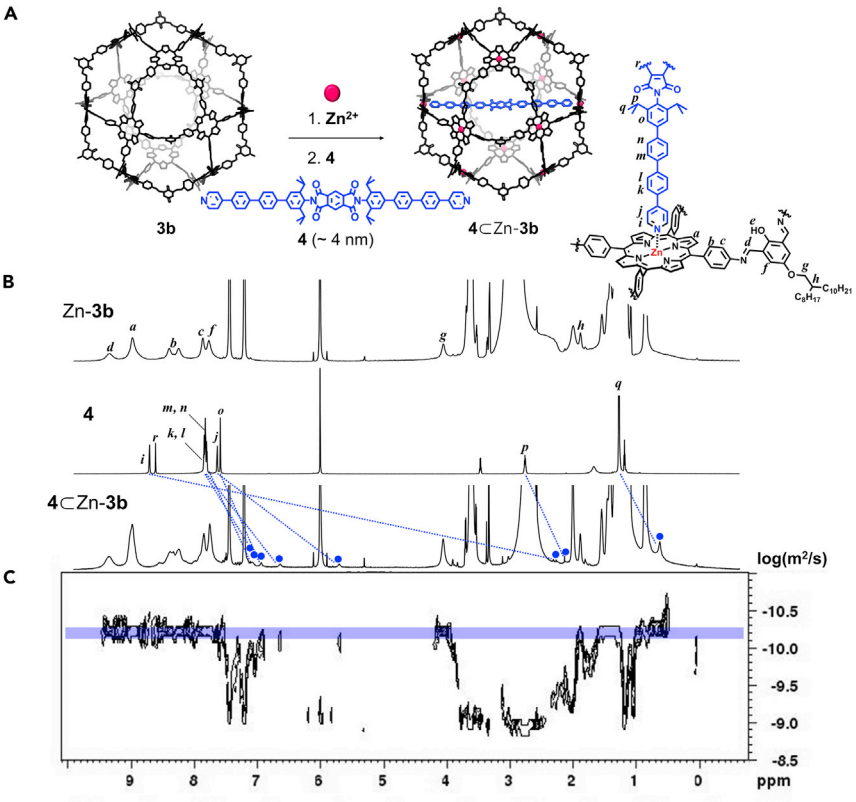

Figure 4. Encapsulation of a Guest Molecule

(A) Schematic illustration of insertion of a linear guest molecule **4** within Zn-**3b**.

(B) ^{1}H NMR spectra of Zn-**3b**, **4**, and **4**⊂Zn-**3b**.

(C) DOSY NMR spectrum of **4**⊂Zn-**3b**.

linkers and/or metal clusters, which would otherwise be difficult to place in the desired proximity. Additionally, suitable derivatives of **3b**, can also be potentially applied for the encapsulation of intriguing large guest molecules, such as proteins, homogeneous catalysis, and building superstructures with an addition of external linkers. Work along these lines is in progress.

CONCLUSION

The construction of molecularly precise gigantic spherical architectures has been a long-standing challenge for chemists. Toward the realization of such a goal, we made numerous attempts to program a larger number of porphyrin units (more than six) to assemble into predesigned hollow multiporphyrin-based architectures. However, we faced a number of hurdles, including solubility issues, formation of intractable polymeric products, and entropically favorable formation of smaller-sized cages. Finally, to construct well-defined, 3D gigantic porphyrin cages, we rationally designed $P_{12}L_{24}$ from a combination of rigid square-shaped porphyrin monomers and suitable complementary vertex linkers. Confinement of 12 porphyrin moieties into well-ordered, nanoscale spherical cages can be considered as a significant addition to not only the family of multiporphyrin-based architectures but also to dynamic covalent supramolecules. X-ray crystallography suggests that **3a** is the largest void containing pure organic cage reported so far. The reported gigantic porphyrinic cage mimics the basic structure of the COPII, which mediates cargo transport between distinct cellular compartments. Consequently, we anticipate

that **3a** and **3b** can be exploited as pure organic cages, and also that their applications can be expanded beyond the photophysical properties of an artificial light-harvesting complex and *in vitro* cargo trafficking systems. One of the most intriguing applications can be the protective encapsulation of large functional guest molecules, such as proteins, through host-guest interactions. However, one needs to synthesize such large organic cages, which are stable under biological conditions. We are currently working toward realizing such goals.

EXPERIMENTAL PROCEDURES

Full experimental procedures are provided in the Supplemental Information.

RESOURCE AVAILABILITY

Lead Contact

Further information and requests for resources and reagents should be directed to and will be fulfilled by the Lead Contact, Kimoon Kim (kkim@postech.ac.kr)

Materials Availability

All unique/stable reagents generated in this study are available from the Lead Contact with a completed Materials Transfer Agreement.

Data and Code Availability

The **3a** structures reported in this article have been deposited in the Cambridge Crystallographic Data Center under accession number CCDC: 2035605.

SUPPLEMENTAL INFORMATION

Supplemental Information can be found online at https://doi.org/10.1016/j.chempr.2020.10.002.

ACKNOWLEDGMENTS

This work was supported by the Institute for Basic Science (IBS) [IBS-R007-D1 and IBS-R010-A1]. X-ray crystallography experiments with synchrotron radiation were performed at the Pohang Accelerator Laboratory (PLS-II BL11C Micro-MX, BL2D SMC, BL6D C&S UNIST-PAL beamlines).

AUTHOR CONTRIBUTIONS

J.K., Y.K., and K.K. conceived and designed the experiments. J.K., I.K., Y.K., H.S., A.D., and H.L. performed the experiments and analyzed the data. J.K., I.K., Y.K., and I.-C.H. carried out single crystal X-ray analyses. Y.K., I.K., and R.D.M. performed photocatalysis. W.H. measured AFM. I.K. and Y.H.K. performed 2D NMR analyses. D.C., S.K., and M.-H.B. performed computations. J.K., R.D.M., and K.K. wrote the paper. All authors discussed the results and commented on the manuscript.

DECLARATION OF INTERESTS

The authors declare no competing interests.

Received: April 17, 2020
Revised: June 19, 2020
Accepted: October 2, 2020
Published: October 27, 2020

REFERENCES

1. Papageorgiou, G.C., and Govindjee. (2007). Chlorophyll A Fluorescence: A Signature of Photosynthesis (Springer Science & Business Media).
2. Zlotnick, A. (1994). To build a virus capsid: An equilibrium model of the self assembly of polyhedral protein complexes. J. Mol. Biol. *241*, 59–67.
3. Grimes, J.M., Burroughs, J.N., Gouet, P., Diprose, J.M., Malby, R., Ziéntara, S., Mertens, P.P.C., and Stuart, D.I. (1998). The atomic structure of the bluetongue virus core. Nature *395*, 470–478.
4. Lawson, D.M., Artymiuk, P.J., Yewdall, S.J., Smith, J.M.A., Livingstone, J.C., Treffry, A., Luzzago, A., Levi, S., Arosio, P., Cesareni, G., et al. (1991). Solving the structure of human H ferritin by genetically engineering intermolecular crystal contacts. Nature *349*, 541–544.
5. Stagg, S.M., Gürkan, C., Fowler, D.M., LaPointe, P., Foss, T.R., Potter, C.S., Carragher, B., and Balch, W.E. (2006). Structure of the sec13/31 COPII coat cage. Nature *439*, 234–238.
6. Stagg, S.M., Lapointe, P., Razvi, A., Gürkan, C., Potter, C.S., Carragher, B., and Balch, W.E. (2008). Structural basis for cargo regulation of COPII coat assembly. Cell *134*, 474–484.
7. Faini, M., Beck, R., Wieland, F.T., and Briggs, J.A.G. (2013). Vesicle coats: structure, function, and general principles of assembly. Trends Cell Biol. *23*, 279–288.
8. Wikoff, W.R., Liljas, L., Duda, R.L., Tsuruta, H., Hendrix, R.W., and Johnson, J.E. (2000). Topologically linked protein rings in the bacteriophage HK97 capsid. Science *289*, 2129–2133.
9. Takahashi, R., and Kobuke, Y. (2003). Hexameric macroring of gable-porphyrins as a light-harvesting antenna mimic. J. Am. Chem. Soc. *125*, 2372–2373.
10. Nakamura, Y., Aratani, N., and Osuka, A. (2007). Cyclic porphyrin arrays as artificial photosynthetic antenna: synthesis and excitation energy transfer. Chem. Soc. Rev. *36*, 831–845.
11. Aratani, N., Kim, D., and Osuka, A. (2009). Discrete cyclic porphyrin arrays as artificial light-harvesting antenna. Acc. Chem. Res. *42*, 1922–1934.
12. Tanaka, T., and Osuka, A. (2015). Conjugated porphyrin arrays: synthesis, properties and applications for functional materials. Chem. Soc. Rev. *44*, 943–969.
13. Li, W.-S., and Aida, T. (2009). Dendrimer porphyrins and phthalocyanines. Chem. Rev. *109*, 6047–6076.
14. Gao, W.Y., Chrzanowski, M., and Ma, S. (2014). Metal-metalloporphyrin frameworks: a resurging class of functional materials. Chem. Soc. Rev. *43*, 5841–5866.
15. Huh, S., Kim, S.-J., and Kim, Y. (2016). Porphyrinic metal-organic frameworks from custom-designed porphyrins. CrystalEngComm. *18*, 345–368.
16. Feng, X., Liu, L., Honsho, Y., Saeki, A., Seki, S., Irle, S., Dong, Y., Nagai, A., and Jiang, D. (2012). High-rate charge-carrier transport in porphyrin covalent organic frameworks: switching from hole to electron to ambipolar conduction. Angew. Chem. Int. Ed. Engl. *51*, 2618–2622.
17. Lin, G., Ding, H., Chen, R., Peng, Z., Wang, B., and Wang, C. (2017). 3D porphyrin-based covalent organic frameworks. J. Am. Chem. Soc. *139*, 8705–8709.
18. Bols, P.S., and Anderson, H.L. (2018). Template-directed synthesis of molecular nanorings and cages. Acc. Chem. Res. *51*, 2083–2092.
19. Hwang, I.W., Kamada, T., Ahn, T.K., Ko, D.M., Nakamura, T., Tsuda, A., Osuka, A., and Kim, D. (2004). Porphyrin boxes constructed by homochiral self-sorting assembly: optical separation, exciton coupling, and efficient excitation energy migration. J. Am. Chem. Soc. *126*, 16187–16198.
20. Bahng, H.W., Kim, P., Sung, Y.M., Maeda, C., Osuka, A., and Kim, D. (2012). Molecular engineering and solvent dependence of excitation energy hopping in self-assembled porphyrin boxes. Chem. Commun. *48*, 4181–4183.
21. Mosquera, J., Szyszko, B., Ho, S.K.Y., and Nitschke, J.R. (2017). Sequence-selective encapsulation and protection of long peptides by a self-assembled FeII8L6 cubic cage. Nat. Commun. *8*, 14882.
22. Wiester, M.J., Ulmann, P.A., and Mirkin, C.A. (2011). Enzyme mimics based upon supramolecular coordination chemistry. Angew. Chem. Int. Ed. Engl. *50*, 114–137.
23. Benke, B.P., Aich, P., Kim, Y., Kim, K.L., Rohman, M.R., Hong, S., Hwang, I.C., Lee, E.H., Roh, J.H., and Kim, K. (2017). Iodide-selective synthetic ion channels based on shape-persistent organic cages. J. Am. Chem. Soc. *139*, 7432–7435.
24. Tsuda, A., Nakamura, T., Sakamoto, S., Yamaguchi, K., and Osuka, A. (2002). A self-assembled porphyrin box from meso-meso-linked bis[5-p-pyridyl-15-(3,4-di-octyl-oxyphenyl)porphyrinato zinc(II)]. Angew. Chem. Int. Ed. Engl. *41*, 2817–2821.
25. Johnston, M.R., and Latter, M.J. (2005). Capsules, cages and three-dimensional hosts: self-assembly of complementary monomers. Supramol. Chem. *17*, 595–607.
26. Tsuda, A., Hu, H., Watanabe, R., and Aida, T. (2003). π-Conjugated multiporphyrin box via self-assembly of an ethynylene-bridged zinc porphyrin dimer. J. Porphyrins Phthalocyanines *07*, 388–393.
27. Aimi, J., Nagamine, Y., Tsuda, A., Muranaka, A., Uchiyama, M., and Aida, T. (2008). "Conformational" solvatochromism: spatial discrimination of nonpolar solvents by using a supramolecular box of a π-conjugated zinc bisporphyrin rotamer. Angew. Chem. Int. Ed. Engl. *47*, 5153–5156.
28. Rizzuto, F.J., and Nitschke, J.R. (2017). Stereochemical plasticity modulates cooperative binding in a CoII12L6 cuboctahedron. Nat. Chem. *9*, 903–908.
29. Meng, W., Breiner, B., Rissanen, K., Thoburn, J.D., Clegg, J.K., and Nitschke, J.R. (2011). A self-assembled M8L6 cubic cage that selectively encapsulates large aromatic guests. Angew. Chem. Int. Ed. Engl. *50*, 3479–3483.
30. Brenner, W., Ronson, T.K., and Nitschke, J.R. (2017). Separation and selective formation of fullerene adducts within an M(II)(8)L(6) cage. J. Am. Chem. Soc. *139*, 75–78.
31. Rizzuto, F.J., Wood, D.M., Ronson, T.K., and Nitschke, J.R. (2017). Tuning the redox properties of fullerene clusters within a metal-organic capsule. J. Am. Chem. Soc. *139*, 11008–11011.
32. Wood, D.M., Meng, W., Ronson, T.K., Stefankiewicz, A.R., Sanders, J.K.M., and Nitschke, J.R. (2015). Guest-induced transformation of a porphyrin-edged FeII4L6 capsule into a CuIFeII2L4 fullerene receptor. Angew. Chem. Int. Ed. Engl. *54*, 3988–3992.
33. Struch, N., Bannwarth, C., Ronson, T.K., Lorenz, Y., Mienert, B., Wagner, N., Engeser, M., Bill, E., Puttreddy, R., Rissanen, K., et al. (2017). An octamer metallosupramolecular cage designed to exhibit spin-crossover behavior. Angew. Chem. Int. Ed. Engl. *56*, 4930–4935.
34. Percástegui, E.G., Mosquera, J., and Nitschke, J.R. (2017). Anion exchange renders hydrophobic capsules and cargoes water-soluble. Angew. Chem. Int. Ed. Engl. *56*, 9136–9140.
35. Durot, S., Taesch, J., and Heitz, V. (2014). Multiporphyrinic cages: architectures and functions. Chem. Rev. *114*, 8542–8578.
36. Inomata, T., and Konishi, K. (2003). Gold nanocluster confined within a cage: template-directed formation of a hexaporphyrin cage and its confinement capability. Chem. Commun. 1282–1283.
37. Taesch, J., Heitz, V., Topić, F., and Rissanen, K. (2012). Templated synthesis of a large and flexible covalent porphyrinic cage bearing orthogonal recognition sites. Chem. Commun. *48*, 5118–5120.
38. Cremers, J., Haver, R., Rickhaus, M., Gong, J.Q., Favereau, L., Peeks, M.D., Claridge, T.D.W., Herz, L.M., and Anderson, H.L. (2018). Template-directed synthesis of a conjugated zinc porphyrin nanoball. J. Am. Chem. Soc. *140*, 5352–5355.
39. Tozawa, T., Jones, J.T.A., Swamy, S.I., Jiang, S., Adams, D.J., Shakespeare, S., Clowes, R., Bradshaw, D., Hasell, T., Chong, S.Y., et al. (2009). Porous organic cages. Nat. Mater. *8*, 973–978.
40. Slater, A.G., and Cooper, A.I. (2015). Function-led design of new porous materials. Science *348*, aaa8075.
41. Hasell, T., and Cooper, A.I. (2016). Porous organic cages: soluble, modular and molecular pores. Nat. Rev. Mater. *1*, 16053.
42. Slater, A.G., Reiss, P.S., Pulido, A., Little, M.A., Holden, D.L., Chen, L., Chong, S.Y., Alston, B.M., Clowes, R., Haranczyk, M., et al. (2017).

Computationally guided synthetic control over pore size in isostructural porous organic cages. ACS Cent. Sci. *3*, 734–742.

43. Mastalerz, M. (2008). One-pot synthesis of a shape-persistent endo-functionalised nano-sized adamantoid compound. Chem. Commun. 4756–4758.

44. Elbert, S.M., Rominger, F., and Mastalerz, M. (2014). Synthesis of a rigid C3v-symmetric tris-salicylaldehyde as a precursor for a highly porous molecular cube. Chem. Eur. J. *20*, 16707–16720.

45. Mastalerz, M. (2010). Shape-persistent organic cage compounds by dynamic covalent bond formation. Angew. Chem. Int. Ed. Engl. *49*, 5042–5053.

46. Zhang, G., Presly, O., White, F., Oppel, I.M., and Mastalerz, M. (2014). A permanent mesoporous organic cage with an exceptionally high surface area. Angew. Chem. Int. Ed. Engl. *53*, 1516–1520.

47. Zhang, G., and Mastalerz, M. (2014). Organic cage compounds – from shape-persistency to function. Chem. Soc. Rev. *43*, 1934–1947.

48. Ono, K., Johmoto, K., Yasuda, N., Uekusa, H., Fujii, S., Kiguchi, M., and Iwasawa, N. (2015). Self-assembly of nanometer-sized boroxine cages from diboronic acids. J. Am. Chem. Soc. *137*, 7015–7018.

49. Mastalerz, M. (2018). Porous shape-persistent organic cage compounds of different size, geometry, and function. Acc. Chem. Res. *51*, 2411–2422.

50. Rue, N.M., Sun, J., and Warmuth, R. (2011). Polyimine container molecules and nanocapsules. Isr. J. Chem. *51*, 743–768.

51. Skowronek, P., Warżajtis, B., Rychlewska, U., and Gawroński, J. (2013). Self-assembly of a covalent organic cage with exceptionally large and symmetrical interior cavity: the role of entropy of symmetry. Chem. Commun. *49*, 2524–2526.

52. Belowich, M.E., and Stoddart, J.F. (2012). Dynamic imine chemistry. Chem. Soc. Rev. *41*, 2003–2024.

53. Hong, S., Rohman, M.R., Jia, J., Kim, Y., Moon, D., Kim, Y., Ko, Y.H., Lee, E., and Kim, K. (2015). Porphyrin boxes: rationally designed porous organic cages. Angew. Chem. Int. Ed. Engl. *54*, 13241–13244.

54. Smith, P.T., Benke, B.P., Cao, Z., Kim, Y., Nichols, E.M., Kim, K., and Chang, C.J. (2018). Iron porphyrins embedded into a supramolecular porous organic cage for electrochemical CO2 reduction in water. Angew. Chem. Int. Ed. Engl. *57*, 9684–9688.

55. Kim, Y., Koo, J., Hwang, I.-C., Mukhopadhyay, R.D., Hong, S., Yoo, J., et al. (2018). Rational design and construction of hierarchical superstructures using shape-persistent organic cages: porphyrin box-based metallosupramolecular assemblies. J. Am. Chem. Soc. *140*, 14547–14551.

56. Mukhopadhyay, R.D., Kim, Y., Koo, J., and Kim, K. (2018). Porphyrin boxes. Acc. Chem. Res. *51*, 2730–2738.

57. Yu, X., Wang, B., Kim, Y., Park, J., Ghosh, S., Dhara, B., Mukhopadhyay, R.D., Koo, J., Kim, I., Kim, S., et al. (2020). Supramolecular fullerene tetramers concocted with porphyrin boxes enable efficient charge separation and delocalization. J. Am. Chem. Soc. *142*, 12596–12601.

58. Tominaga, M., Suzuki, K., Kawano, M., Kusukawa, T., Ozeki, T., Sakamoto, S., Yamaguchi, K., and Fujita, M. (2004). Finite, spherical coordination networks that self-organize from 36 small components. Angew. Chem. Int. Ed. Engl. *43*, 5621–5625.

59. Suzuki, K., Tominaga, M., Kawano, M., and Fujita, M. (2009). Self-assembly of an M6L12 coordination cube. Chem. Commun. 1638–1640.

60. Sun, Q.F., Iwasa, J., Ogawa, D., Ishido, Y., Sato, S., Ozeki, T., Sei, Y., Yamaguchi, K., and Fujita, M. (2010). Self-assembled M24L48 polyhedra and their sharp structural switch upon subtle ligand variation. Science *328*, 1144–1147.

61. Fujita, D., Yokoyama, H., Ueda, Y., Sato, S., and Fujita, M. (2015). Geometrically restricted intermediates in the self-assembly of an M12L24 cuboctahedral complex. Angew. Chem. Int. Ed. Engl. *54*, 155–158.

62. Fujita, D., Ueda, Y., Sato, S., Mizuno, N., Kumasaka, T., and Fujita, M. (2016). Self-assembly of tetravalent Goldberg polyhedra from 144 small components. Nature *540*, 563–566.

63. Fujita, D., Ueda, Y., Sato, S., Yokoyama, H., Mizuno, N., Kumasaka, T., and Fujita, M. (2016). Self-assembly of M30L60 icosidodecahedron. Chem *1*, 91–101.

64. Xie, T.-Z., Guo, K., Guo, Z., Gao, W.-Y., Wojtas, L., Ning, G.-H., Huang, M., Lu, X., Li, J.-Y., Liao, S.-Y., et al. (2015). Precise molecular fission and fusion: quantitative self-assembly and chemistry of a metallo-cuboctahedron. Angew. Chem. Int. Ed. Engl. *54*, 9224–9229.

65. Day, G.M., and Cooper, A.I. (2018). Energy-structure-function maps: cartography for materials discovery. Adv. Mater. *30*, e1704944.

66. Rousseaux, S.A.L., Gong, J.Q., Haver, R., Odell, B., Claridge, T.D.W., Herz, L.M., and Anderson, H.L. (2015). Self-assembly of Russian doll concentric porphyrin nanorings. J. Am. Chem. Soc. *137*, 12713–12718.